6314 J. Med. Chem. 2009, 52, 6314–6323
DOI: 10.1021/jm9006752

Journal of Medicinal Chemistry Article

Aminoimidazoles as Potent and Selective Human β-Secretase (BACE1) Inhibitors†

Michael S. Malamas,*,† Jim Erdei,† Iwan Gunawan,† Keith Barnes,‡ Matthew Johnson,‡ Yu Hui,‡ Jim Turner,§ Yun Hu,§ Erik Wagner,§ Kristi Fan,† Andrea Olland,∥ Jonathan Bard,§ and Albert J. Robichaud†

†Department of Chemical Sciences, Wyeth Research, CN 8000, Princeton, New Jersey 08543-8000, ‡Albany Molecular Research, Albany, New York, §Neuroscience, Wyeth Research, CN 8000, Princeton, New Jersey 08543-8000, and ∥Department of Chemical Sciences, Wyeth Research, 200 Cambridge Park Drive, Cambridge, Massachusetts 02140

Received May 20, 2009

The identification of small molecule aminoimidazoles as potent and selective human β-secretase inhibitors is reported. These analogues demonstrate low nannomolar potency for BACE1 in a FRET assay, exhibit comparable activity in a cell-based (ELISA) assay, and show >100× selectivity for the other structurally related aspartyl proteases BACE2, cathepsin D, renin, and pepsin. Our design strategy was supported by molecular modeling studies based on the cocrystal structure of the HTS-hit **3** in the BACE1 active site. These strategies enabled us to integrate pyridine and pyrimidine groups on **3** extending deep into the S3 region of the BACE1 binding pocket and enhancing the ligand's potency. Compound (*R*)-**37** displayed an IC_{50} value for BACE1 of 20 nM, cellular activity of 90 nM, and >100-fold selectivity over related aspartyl proteases. Acute oral administration of (*R*)-**37** at 30 mg/kg resulted in a significant 71% reduction of plasma $A\beta_{40}$ measured at the 6 h time point in a Tg2576 mouse model ($p < 0.001$).

Introduction

Alzheimer's disease (AD[a]) is a progressive, degenerative disease of the brain and the leading cause of dementia. At the early stage, AD is associated with gradual loss of cognition (memory, reasoning, orientation, and judgment) that ultimately leads to deterioration of cognitive and behavioral functions and death. There exists a plethora of genetic and pathological evidence indicating that the formation of β-amyloid plaques in the brain is a major pathological event in the progression of AD.[1,2] β-Amyloid deposits are predominately aggregates of the Aβ peptides (Aβ, 39−43 residues) resulting from the endoproteolysis of the amyloid precursor protein (APP), a type I membrane-bound protein of 770 amino acids in length.[3,4] Aβ peptides result from the sequential cleavage of APP, first at the N-terminus by β-secretase enzyme (β-site APP cleaving enzyme, BACE1),[5,6] followed at the C-terminus by one or more γ-secretase complexes (intramembrane aspartyl proteases),[7] as part of the β-amyloidogenic pathway. Thus, processes that limit the accumulation of Aβ production deposits by preventing formation, inhibiting aggregation, and/or enhancing clearance may offer effective treatments for AD. Since β-secretase mediated cleavage of APP is the first step of the amyloidogenic pathway, BACE1 inhibition is an important therapeutic approach for treating AD by diminishing Aβ peptide formation in AD patients.

The initial disclosed work in the design of BACE1 inhibitors was concentrated on peptidic substrate transition-state mimic inhibitors.[8] These ligands showed excellent low nanomolar inhibitory potency for BACE1 but were not suitable as CNS drugs because of their poor pharmacokinetic properties. More recently, structure-based drug design approaches have led to the generation of less-peptidic second-generation inhibitors.[9−16] Tang (Oklahoma Medical Research Foundation) and Ghosh (University of Illinois) have pioneered the evolution of substrate-based inhibitors with OM99-2 (**1**, Figure 1), a highly potent BACE1 inhibitor (IC_{50} = 1.6 nM). The newest generation BACE1 inhibitors are low molecular weight molecules with excellent cell permeability, have little or no peptidic character, and possess enhanced pharmacokinetic profiles.[17−22] Recent reports have revealed the application of fragment-based lead generation and computational approaches to the design of potent small-size BACE1 inhibitors.[23−26] Also, particularly notable is a report on a small-molecule ligand with a novel acylguanidine pharmacophore 2 (IC_{50} = 110 nM; Figure 1) as a BACE1 inhibitor.[27]

In this paper, we report the design and synthesis of potent and selective small-molecule BACE1 inhibitors, which originated from the HTS hit **3** (Figure 1). Compound **3** was identified through a FRET assay screen of our in-house sample collection. It had weak in vitro potency for BACE1 with an IC_{50} value of 38 μM and demonstrated weak cell-based ELISA potency with an EC_{50} value of 27 μM. The development of this lead series followed a traditional SAR approach and was supported by X-ray structures of BACE1 cocrystallized with various ligands and molecular modeling to expedite the discovery of potent compounds. An X-ray crystal

*To whom correspondence should be addressed. Telephone: 732-274-4428. Facsimile: 732-274-4505. E-mail: malamam@wyeth.com.

†The atomic coordinates of the PDE10A crystal structure for compound **3** (3IGB) have been deposited in the Protein Data Bank, Research Collaboratory for Structural Bioinformatics, Rutgers University, New Brunswick, New Jersey.

[a] Abbreviations: AD, Alzheimer's disease; Aβ, β-amyloid peptide; APP, β-amyloid precursor protein; BACE, β-site β-amyloid precursor protein cleaving enzyme; FRET, fluorescence resonance energy transfer; Abz, *o*-aminobenzoic acid; Dpa, 3-(2,4-dinitrophenyl)- L-2,3-diaminopropionic amide; Dnp, 6-(2,4-dinitrophenyl); MOCAc, 7-methoxycoumarin-4-yl; EDANS, 5-[(2-aminoethyl)amino]naphthalene-1-sulfonic acid; DABCYL, 4,4-dimethylaminoazobenzene-4′-carboxylic acid; ELISA, enzyme-linked immune sandwich assay; CHO, Chinese hamster ovary.

 Published on Web 09/16/2009

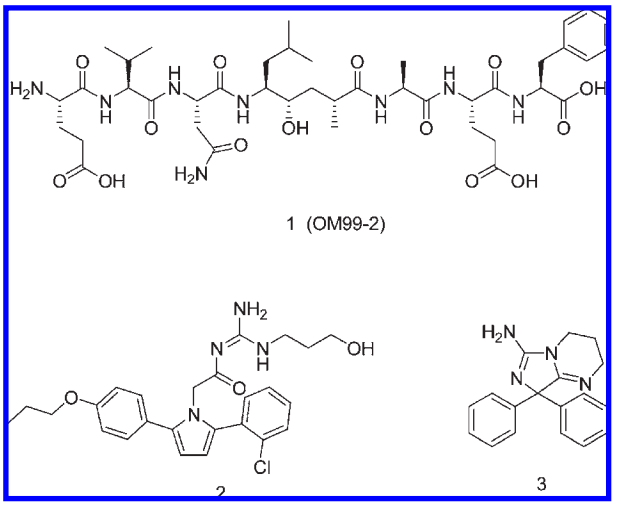

Figure 1

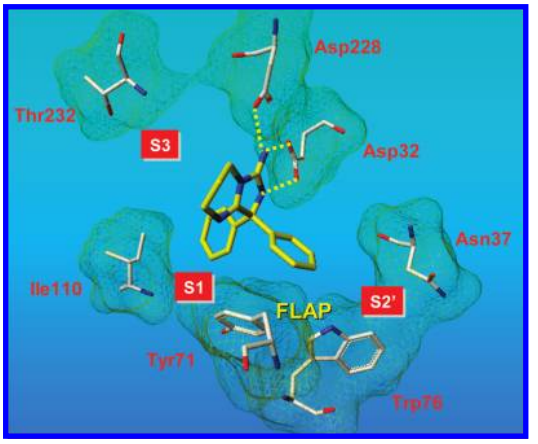

Figure 2. Crystal structure of BACE1 complexed with **3**, highlighting the three key hydrogen-bonding interactions between the catalytic aspartic acids Asp32 and Asp228 and the aminoimidazole moiety.

structure of **3** in a complex with BACE1 was resolved to 2.3 Å (Figure 2), defining the three-dimensional structure of the enzyme and its interactions with the inhibitor. It can be seen from the figure that compound **3** occupies the center of the rather large BACE1 binding pocket (S1, S2′ regions) in an orientation where the aminoimidazole portion of the ligand directly interacts with both catalytic-site aspartic acids (Asp32 and Asp228) via a hydrogen-bonding network. The structure also shows that the S3 region is directly accessible by suitable substitution of the moiety occupying the S1 pocket, indicating an opportunity to build off the phenyl moiety into this S3 region and improve binding affinity. We have initially concentrated our synthetic efforts exploring this region as well as optimization of the proximal S2′ region that has resulted in the identification of low nanomolar BACE1 inhibitors. The structure−activity relationship evolution around the HTS-hit **3** will be the central focus of this report.

Chemistry

The compounds shown in Tables 1−3 were synthesized according to the general Schemes 1 and 2. Commercially available benzaldehydes **4** were converted to cyanohydrins **5** in good yields by treatment with sodium cyanide and sodium bisulfite. Treatment of **5** with ethanol under acidic conditions gave imidates **6**, which upon cyclization with propane-1,3-diamine furnished compounds **7** in 67% overall yield. Oxidation of **7** with manganese dioxide produced the requisite ketones **8** in 85% yield. Treatment of **8** with a suitable Grignard reagent **9** afforded the adducts **10**, which could then be converted to the chlorides **11** with thionyl chloride. Chlorides **11** were reacted with ammonia to afford amines **12** in 22% yield over the three steps. Subsequent treatment of **12** with cyanogen bromide gave the rearranged bicyclic compounds **13** in a variable 5−9% conversion. Palladium-catalyzed cross-coupling[28,29] reaction of advanced intermediates **13** with any number of heteroarylboronic acids (Suzuki coupling) or heteroaryltrialkyl/-triaryl stannanes (Stille coupling) in the presence of Pd(0) or Pd(II) catalysts produced the desired products **14** in good yields.

During the course of the exploration of the SAR, the need for a more directed and higher yielding approach to advanced compounds was desired. Because of the variable and poor yielding steps for some of the required substitution patterns, an alternative approach was developed. Furthermore, this approach allowed for the facile preparation of heterocyclic variants of the aminoimidazole bicyclic core (Table 4) not readily assessable from the initial approach.

To that end, as shown in Scheme 2, benzonitrile derivatives **15** were treated with the desired Grignard reagents **16** to afford imines **17**, which were immediately reduced with sodium borohydride to furnish the biarylamines **18** in 34% overall yield. Treatment of **18** with thiophosgene in the presence of sodium bicarbonate gave isothiocyanates **19**, which were subsequently treated with potassium *tert*-butoxide and carbon disulfide to yield the rearranged 1,3-thiazolidine-2,5-dithiones **20** in an excellent 92% conversion. Cyclization of **20** with various diamines **21** furnished the bicyclic intermediates **22** in 56% yield. Treatment of **22** with *tert*-butyl hydroperoxide and ammonium hydroxide furnished the desired aminoimidazole core derivatives **23** in an improved and more efficient manner (fewer synthetic steps) than the previous approach (Scheme 1). Palladium-catalyzed cross-coupling reactions of **23** with heteroarylboronic acids or heteroaryltrialkyl/-triaryl stannanes as described earlier afforded the desired products **24** in similar fashion and yields.

Results and Discussion

The primary screening assay utilized for the program was a homogeneous, continuous fluorescence resonance energy transfer (FRET) protocol representing competitive inhibition for BACE1, BACE2, cathepsin D, pepsin, and renin activities.[30] The BACE1 and BACE2 affinities were based on the cleavage of peptide substrate Abz-SEVNLDAEFR-Dpa (Swedish substrate), while peptide substrate MOCAc-GKPILFFRLK (Dnp)-D-R-NH_2 was used for cathepsin D and pepsin, and peptide substrate RE(EDANS)-IHPFHLVIHTK(DABCYL)-R for renin. Kinetic rates were calculated and IC_{50} values were determined by fitting the % inhibition as a function of compound concentration to the Hill equation, $y = [(BKn) + (100 \times xn)]/(Kn + xn)$. We have routinely screened all prepared compounds for BACE1, BACE2, and cathepsin D inhibition, and only selected compounds were assayed in the pepsin and renin screens, based on their meeting the screening protocol for affinity to the target, and are reported in Tables 1−5.

The cell-based Aβ inhibition (Aβ_{40} or Aβ_{42}) of the potential inhibitors was assessed in an enzyme-linked immune sandwich assay (ELISA) in Chinese hamster ovary (CHO) cells,

Table 1. Aminoimidazoles

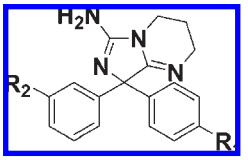

compd	R_1	R_2	IC_{50} (μM)[a] BACE1	BACE2	cathepsin D	ELISA EC_{50} (μM)[a]
3	H	H	38.0	38.3 ± 3.2	16% at 200 μM	16 ± 3.0
25	H	CF_3	21.9	30.1	28% at 100 μM	5.1 ± 0.8
26	H	OMe	20.3	24.4	22% at 100 μM	20.9 ± 4.3
27	H	*tert*-butyl	30.2	21% at 100 μM	150.1	3.0 ± 1.7
28	H	CH_2Ph	5.3 ± 1.3	10.9	52.5 ± 10	5.1 ± 1.1
29	H	CH_2Ph-4OMe	7.1 ± 12.2	22.4	24.9 ± 6.7	5.1 ± 1.8
30	H	CH_2Ph-4F	8.2	7.0	9.2 ± 0.5	4.6 ± 1.6
31	OCF_3	Br	2.6 ± 0.2	39% at 2.5 μM	47.4	1.6 ± 0.2
32	OCF_3	$CH_2CH_2CH_3$	1.43	25% at 12.5 μM	93.7	2.1 ± 0.2
33	OCF_3	CH_2CH_2-cyclopropane	0.21	3.78	16.44	0.95 ± 0.06

[a] IC_{50} and EC_{50} values are the mean of at least two experiments ± SD. Values without SD are for a single determination only.

Table 2. Heteoarylaminoimidazoles

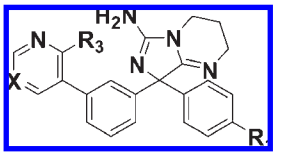

compd	R_1	R_3	X	IC_{50} (μM)[a] BACE1	BACE2	cathepsin D	ELISA EC_{50} (μM)[a]
34	OMe	H	N	0.1 ± 0.02	16.18	69.5	1.4 ± 0.04
35	OCF_3	H	N	0.1 ± 0.01	16.7	78.7 ± 1.8	0.19 ± 0.1
(*R*)-**35**	OCF_3	H	N	0.034 ± 0.004	10.7 ± 0.91	36.2 ± 3.2	0.08 ± 0.02
(*S*)-**35**	OCF_3	H	N	0.79	12% at 12.5 μM	29% at 100 μM	2.56 ± 0.4
36	OMe	F	C	0.07 ± 0.02	6.6	16.5	1.63 ± 0.3
37	OCF_3	F	C	0.06	11.4	18.1	0.3 ± 0.1
(*R*)-**37**	OCF_3	F	C	0.02 ± 0.005	3.6 ± 0.7	6.9 ± 1.6	0.09 ± 0.04
(*S*)-**37**	OCF_3	F	C	0.37	27% at 12.5 μM	56.9	5.1 ± 1.3

[a] IC_{50} and EC_{50} values are the mean of at least two experiments ± SD. Values without SD are for a single determination only.

recombinantly expressing human wild-type APP (CHO-wt). The concentration at which the cellular production of $A\beta_{40}$ or $A\beta_{42}$ was reduced by 50% (EC_{50}) was determined and reported in the tables. Potential compound toxicity was assessed via mitochondrial function using MTS readout (MTS kit from Promega); values are represented as LD_{50} or the dose of compound that resulted in 50% of control signal. MTS data will be discussed only for compounds indicating toxicity concerns.

As previously described, high-throughput screening hit imidazole **3** (Figure 1) was successfully cocrystallized with BACE1 (Figure 2). The structure shows that the amino group of the ligand interacts with both aspartic acids (Asp32 and Asp228) and the N3 nitrogen of the imidazole ring with Asp32. Close examination reveals that the catalytic water of the active site is displaced during the protein/ligand interaction. The hairpin loop known as the FLAP is oriented at a more open position over the bound ligand compared with the peptide bound pocket. Furthermore, the **3**/BACE1 structure indicates that the two aryl groups of the ligand extend into the S1 and S2′ regions, making suboptimal interactions with several residues of the binding pocket.

As mentioned earlier, focus was directed at enhancing potency by building into the S3 pocket and improving ligand binding within the S2′ pocket. One can easily notice that the S1 pocket is highly hydrophobic and approximately spherical in shape and that building off the meta-position of the phenyl ring of the ligand would allow for projection directly toward the unoccupied S3 region (Figure 3). Furthermore, the S2′ region contains a rich environment of polar/charged groups (Tyr198 and Arg128; not shown in Figure 3) and is located in proximity to the FLAP region. From the apo BACE1 enzyme crystal structure, it was noted that several water molecules were located in both the S2′ and S3 regions. These offer the potential for analogues of **3** to displace the buried water molecules and form additional hydrogen bonds with the enzyme backbone and enhance ligand binding affinity. Our initial SAR efforts, originating with compound **3**, encompassed many of these potential advantageous substitutions at the S1 and S2′ phenyl groups. It was envisioned that projecting toward the S3 region would maximize ligand/protein contacts and enhance potency. Benzyl analogues **28**−**30** (Table 1), designed to do precisely this, positioned their substituents deep into S3 region (modeling calculations not shown) and

Table 3. Disubstituted Phenyl Analogues

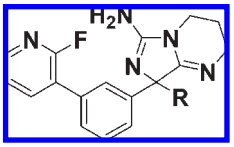

compd	R	BACE1 IC_{50} (uM)[a]	BACE2 IC_{50} (uM)	cathepsin D IC_{50} (uM)
38		0.16	4.4	15.4
39		0.19	10.5	9.6
40	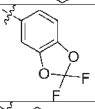	0.74	32%@12.5uM	95.3
41	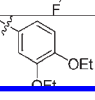	0.08	9.9	63.4

[a] IC_{50} values are the mean of at least two experiments ± SD. Values without SD are for a single determination only.

Scheme 1[a]

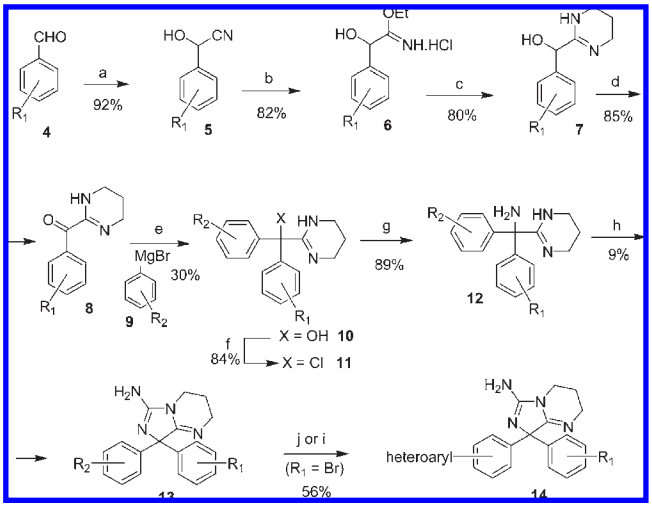

[a] Reagents: (a) NaCN, $NaHSO_3$; (b) EtOH, HCl; (c) H_2N-$(CH_2)_3NH_2$, EtOH; (d) MnO_2, $CHCl_3$; (e) aryl-MgBr,THF; (f) $SOCl_2$, $CHCl_3$; (g) NH_3, MeCN; (h) BrCN, $CHCl_3$; (j) heteroaryl-$B(OH)_2$, $Pd(Ph_3)_4$, K_2CO_3, dioxane, water; (i) heteroaryl-$Sn(Bu)_3$, $PdCl_2(Ph_3)_2$, DMF.

improved the ligand potency about 5-fold. Smaller substituents meant to project into the S3 pocket minimally affected the ligand's affinity (**25**, **26**), as the structure shows these to have less optimal interactions with the S3 pocket. Furthermore, while the bulkier moiety of ligand **27** fills more the S1 hydrophobic pocket, its potency is similar to that of the parent compound (**3**).

Examination of effects of substituting the phenyl ring that projects into the S2′ pocket was also undertaken. After a multitude of substitutions to this pendent phenyl ring were made (not reported) it was discovered that the trifluoromethoxy substituted ligand (entry **31**) shows an approximate 15-fold improvement of BACE1 potency (**31** vs **3**). The trifluoromethoxy moiety was used in further SAR studies looking into alternative and smaller groups projecting into the

Scheme 2[a]

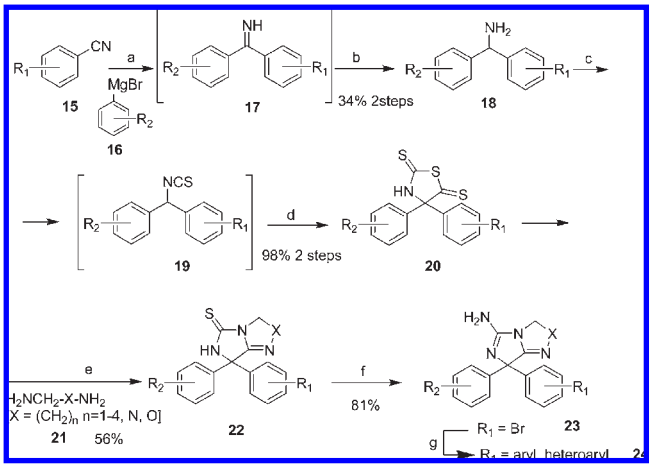

[a] Reagents: (a) Aryl-MgBr,THF; (b) $NaBH_4$, MeOH; (c) $CSCl_2$, $NaHCO_3$, CH_2Cl_2; (d) *t*-BuOK, CS_2, THF; (e) H_2NCH_2-X-NH_2, EtOH; (f) *t*-BuOOH, NH_4OH, MeOH; (g) R_2 = Br, heteroaryl-$B(OH)_2$, $Pd(Ph_3)_4$, K_2CO_3, dioxane, water; or heteroaryl-$Sn(Bu)_3$, $PdCl_2(Ph_3)_2$, DMF.

S3 pocket. By utilization of the trifluoromethoxy substituted phenyl moiety (filling the S2′ pocket), it was discovered that medium chain length alkyl groups (entries **32** and **33**), in deference to the bulkier aryl moieties, allowed for potency enhancement with an overall reduction in ligand bulk. In particular, the cyclopropane analogue (entry **33**) with an IC_{50} value of 210 nM approaches a 180-fold improvement over the initial ligand **3**. The cell-based activity of **33** also tracked well with the molecular binding, with an EC_{50} value of 950 nM in the ELISA assay.

As we advanced the SAR, a closer examination of the specific residues in the S3′ pocket indicated that a heteroatom substituted aryl group may favorably interact with the glycine residue at position 230 of the BACE1 enzyme backbone. Specifically, modeling revealed that introduction of nitrogen at the 3 or 5 position of the aryl moiety would afford enhanced binding. To that end, introduction of a pyrimidine group (Table 2) at the meta-position of the S1 phenyl allowed for the desired extension into the S3 pocket with the added interaction of the nitrogen with the glycine residue. Affirmation of this rational design improvement was the 100 nM potency of ligand **34** for BACE1 with moderate cell-based activity (EC_{50} = 1400 nM). On the basis of the X-ray structures of closely related scaffolds with BACE1 (unpublished data), the subsequent modeling studies indicated that the pyridine or pyrimidine nitrogen interacts with Ser229 through the conserved water at S3 pocket. As a result, the interaction through a water bridge enhances the ligand binding to BACE1. Utilizing the trifluoromethoxyphenyl moiety for the S2′ pocket, as before, afforded compound (*R*)-**35** with excellent ligand potency (IC_{50} = 34 nM; > 150-fold improvement over **31**) and cellular affinity (EC_{50} = 80 nM) for the BACE1 enzyme and the added feature of improved selectivity over the closely related BACE2 (315×), as well as cathepsin D (1065×), renin (> 1470×x), and pepsin (> 2940×) enzymes. The docking of ligand (*R*)-**35** to the X-ray crystal structure of **3** bound to the enzyme revealed that the pyridine nucleus of (*R*)-**35** is oriented deep into the S3 pocket (Figure 4). Furthermore, an investigation of the chiral preference of the racemic mixtures of this class of compounds, once separated, showed a clear preference for

Table 4. Bicyclic Aminoimidazoles

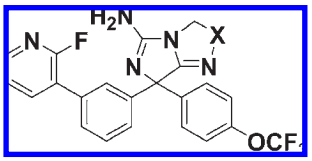

compd	X	IC50 (μM)[a] BACE1	BACE2	cathepsin D	ELISA EC50 (μM)[a]
42	CH_2	0.08 ± 0.01	12.2	10.7	0.25 ± 0.04
37	CH_2CH_2	0.06	11.4	18.1	0.3 ± 0.1
43	$CH_2CH_2CH_2$	0.08 ± 0.01	7.3	10.8	0.3 ± 0.09
44	$CH_2(CH_2)_2CH_2$	0.13 ± 0.02	10.8	11.3	0.9 ± 0.1
45	$CH(CH_3)_2$	0.19 ± 0.03	17.3	33 ± 2.9	1.5 ± 0.2
46	$CH_2O(N)$	0.03 ± 0.006	2.0	2.4	0.2 ± 0.05

[a] IC_{50} values are the mean of at least two experiments ± SD. Values without SD are for a single determination only.

Table 5. Pepsin and Renin Inhibition of Selected Compounds

compd	pepsin, % inhibition at 100 μM	renin, IC50 (μM)[a]
30	6	15% at 50 μM
(*R*)-**35**	12	36% at 50 μM
(*R*)-**37**	13	20.8 ± 1.1
38	18	24% at 50 μM
41	11	14% at 50 μM
46	12	2.04 ± 1

[a] IC_{50} values are the mean of at least two experiments ± SD.

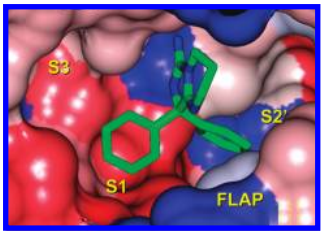

Figure 3. Crystal structure of BACE1 complexed with **3**. Polar/charged residues are shown in blue, and lipophilic residues are shown in red. The aminoimidazole nucleus is oriented toward the catalytic aspartic acids (polar blue region), the S2′-phenyl partially occupies the mixed hydrophobic/lipophilic region, and the S1-phenyl resides are in the middle of the hydrophobic spherical S1-region. The S3 region is unoccupied.

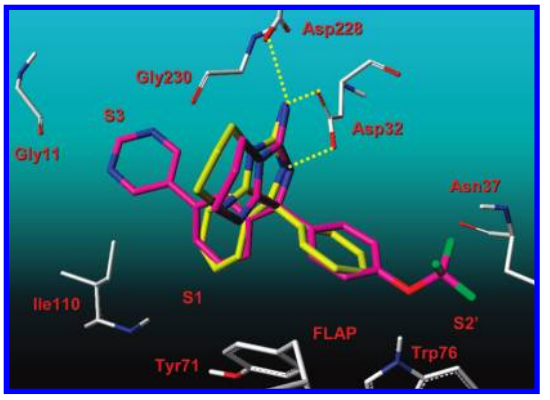

Figure 4. Crystal structure of BACE 1 complexed with **3** (shown in yellow) and ligand **35** (shown in magenta) are overlaid. Key hydrogen-bonding interactions between ligand **3** and protein at the catalytic aspartic acids Asp32 and Asp228 are highlighted with yellow dashed lines. The pyridine nucleus of **35** projects deep into S3 pocket as intended.

the *R*-enantiomer (see (*R*)-**35** vs (*S*)-**35**). This was apparent as the crystal structures and modeling studies bore this out. For the less active enantiomer, one could envision keeping the respective aryl groups in their designed pockets, but in so doing, the bicyclic hydantoin would be flipped into an unfavorable confirmation where the propyl backbone of the six-membered ring would be pressed into the backbone of the active site of the enzyme. An alternative binding pose of ligand **35** within the binding pocket by flipping the respective P1−P3 and P2′ side chains while retaining the interactions of the aminoimidazole moiety with the catalytic aspartic acids results in less interaction with the site compared to (*R*)-**35**. As a result, it could be reflected in the 23-fold potency loss for the (*S*)-**35** enantiomer.

In an effort to reduce the polar surface area of our lead compound, we investigated a heteroaryl group possessing only one nitrogen, namely a pyridine ring, as the desired interaction with the glycine-230 should still be possible. After investigating multiple pyridine analogues substituted with both fluorine and chlorine, we identified the 2-F-3-pyridyl derivative as the best candidate. The reasons for this, although unclear, were not potency driven but centered on subtle metabolic properties which will be the subject of a subsequent disclosure. As with the pyrimidine analogues, the trifluoromethoxyphenyl (S2′) derivative of this 2-F-pyridyl analogue **37** was superior in cellular potency to the corresponding methoxy derivative **36**, and the *R*-enantiomer ((*R*)-**37**) maintained the improved disposition in the active site.

Now with the biaryl appendage occupying the S1−S3 pocket, we focused our efforts on several refined aspects of the ligand binding. Initially, we strived to determine if the 4-alkoxy substituent of the opposing aryl group was indeed the best moiety for the S2′ pocket. Toward that end, a variety of dialkoxy substituents were prepared (Table 3, **38**−**41**) and profiled in the binding assays, and it was apparent that although there are noticeable small differences in potency and selectivity (positive and negative), the overall profile did not change much relative to the 4-alkoxy analogues. In a few of these cases the overall detrimental effect of an additional metabolic liability added to the reasons for choosing the monoalkoxy analogues.

Finally, we looked to the effects of the bicyclic ring system on potency, specifically if we could take advantage of any subtle interactions with the S1′-pocket of the enzyme. A close examination of the X-ray structure of **3** indicated that the

six-member tetrahydropyrimidine ring projects toward this S1′ region, and furthermore, it is solvent exposed without of any obvious contacts of significance in the section of the enzyme backbone. We were intrigued to investigate the effect of size and hydrophilic character of this region of the molecule on BACE1 potency. Toward this goal, we prepared several bicyclic ring arrangements shown in Table 4. Compounds **42**−**46**, together with the parent compound **37**, represent the five- to eight-membered ring systems and showed similar potency and selectivity. The gem-dimethyl substituted analogue **45** exhibited only a marginal loss in potency, while introduction of an oxygen atom into the chain (**46**) resulted in a 2-fold improvement of potency (**46** vs **37**). It had become apparent through research efforts that improvements in potency could not be readily attained in this pocket and further supported the notion that the bicycle extended into solvent space.

To confirm the specificity of these ligands for the BACE1 enzyme, a representative set of compounds were evaluated for inhibition of renin and pepsin aspartyl proteases. As shown in Table 5, all compounds demonstrated weak inhibition for these closely related targets.

To further elucidate the value of these ligands in reducing Aβ, a representative example from this class, (*R*)-**37**, was chosen for further in vivo validation. Dosed at 30 mg/kg po, compound (*R*)-**37** was evaluated in the Tg2576 mouse[32] in vivo model for lowering of plasma and brain Aβ_{40}. Measured at the 6 h time point, (*R*)-**37** showed a significant 71% reduction of plasma Aβ_{40} formation after a single dose ($p < 0.001$). Unfortunately, no significant reduction of brain Aβ_{40} was observed, perhaps because of the limited brain exposure of this compound. Detailed efforts to improve brain exposure of this class of compounds will be reported in due course.

Conclusions

In this report, we have used the cocrystal structure of the HTS-hit **3** in the BACE1 active site, together with molecular modeling studies, to discover highly potent and selective BACE1 inhibitors. The most potent and selective analogues of this series displayed 20−80 nM FRET potency (over 1000-fold improvement vs **3**), comparable cellular activity, and >100-fold selectivity relative to other structurally related aspartyl proteases BACE2, cathepsin D, pepsin, and renin. The addition of either a pyridine or a pyrimidine group on the scaffold of **3** in a manner such that the group extends and occupies the S3 region of the BACE1 binding pocket, not previously accessed with **3**, has significantly contributed to the ligand's potency. The *R*-enantiomer of compound **37** displayed an IC_{50} value for BACE1 of 20 nM, cellular activity of 90 nM, and >100-fold selectivity over the other structurally related aspartyl proteases BACE2, cathepsin D, renin, and pepsin. Acute oral administration of (*R*)-**37** at 30 mg/kg resulted in a significant 71% reduction of plasma Aβ_{40} measured at the 6 h time point in a Tg2576 mouse model ($p < 0.001$). These orally active and selective BACE1 inhibitors will contribute toward the understanding of APP processing, as well as the development of disease-modifying AD therapeutics.

Experimental Section

Chemistry. Melting points were determined in open capillary tubes on a Mel-Temp-II apparatus, and reported uncorrected. ^{1}H NMR spectra were determined in the cited solvent on a Varian Unity or Varian Inova (300−400 MHz) instrument, with tetramethylsilane as an internal standard. Chemical shifts are given in ppm, and coupling constants are in hertz. Splitting patterns are designated as follows: s, singlet; br s, broad singlet; d, doublet; t, triplet; q, quartet; m, multiplet. Mass spectra were recorded on a Micromass LCT, Waters spectrometer. Elemental analyses (C, H, N) were performed on a Perkin-Elmer 240 analyzer, and all compounds are within ±0.4% of theory unless otherwise indicated. HPLC techniques and high resolution mass spectrometry were used to determine the purity of compounds outside the range of the elemental analysis assessment. Purity of all final products was >96% as determined by HPLC and/or combustion analysis. Purity was determined by HPLC analysis using the following protocol: mobile phase A, 10 mM ammonium carbonate in water (pH 9.5); B, 60:50 ACN/MeOH; solvent gradient 85/15 to 5/95 A/B in 2 min, hold 1.25 min, re-equilibrate 0.5 min; flow rate of 1.1 mL/min; column Waters Xbridge C18 2.5 μM, 3.0 mm × 50 mm; temperature 45 °C; detection at 210−370 nM. All products, unless otherwise noted, were purified by "flash chromatography" with use of 220−400 mesh silica gel. Thin-layer chromatography was done on silica gel 60 F-254 (0.25 mm thickness) plates. Visualization was accomplished with UV light and/or 10% phosphomolybdic acid in ethanol. The hydration was determined by the Karl Fischer titration, using a Mitsubishi moisture meter model CA-05. Unless otherwise noted, all materials were obtained commercially and used without further purification. All reactions were carried out under an atmosphere of dried argon or nitrogen.

Representative synthetic protocols of the aminoimidazoles shown in Schemes 1 and 2 are described below.

General Methods for the Preparation of Compounds Illustrated in Scheme 1. 8-(4-*tert*-Butylphenyl)-8-phenyl-2,3,4,8-tetrahydroimidazol[1,5-*a*]pyrimidin-6-amine (13; R_1 = H, R_2 = *tert*-butyl). Preparation of Cyanohydrins 5 (Scheme 1). Step a. (3-Bromo-4-fluorophenyl)(hydroxy)acetonitrile. A mixture of sodium bisulfite (28.3 g, 0.27 mol), water (200 mL), and 3-bromo-4-fluorobenzaldehyde (45.8 g, 0.22 mol) was stirred at 50 °C for 2 h. The mixture was cooled with an ice bath and diluted with ethyl ether, and an aqueous solution of sodium cyanide (12.2 g, 0.25 mmol) was added over a 30 min period. The new mixture was stirred at room temperature for 18 h. Then the organic layer was separated and the aqueous layer was extracted with ethyl ether. The extracts were combined with the organic layer, washed with brine, and dried over $MgSO_4$. Evaporation to dryness afforded 1-(3-bromo-4-fluorophenyl)-1-cyanomethanol as a clear oil, 47.6 g (92% yield): MS *m*/*e* 210 $(M)^+$; ^{1}H NMR (300 MHz, $CDCl_3$) δ 3.1−3.2 (m, 1H), 5.51−5.56 (m, 1H), 7.2−7.31 (m, 1H), 7.44−7.48 (m, 1H), 7.71−7.76 (m, 1H); MS *m*/*e* 210 $(M)^+$.

Step b. Ethyl Mandelimidate Hydrochloride Salt (6; R_1 = H). Into a cold (0 °C) solution of hydroxy(phenyl)acetonitrile (Aldrich, 100 g, 0.75 mol), ethanol (50 mL), and ethyl ether (500 mL) was added dropwise a freshly prepared ether−HCl solution (0.5 mol, 150 mL) over a 30 min period. The reaction mixture was stirred at 0 °C for 6 h and then kept in the refrigerator for 18 h. The resulting suspension was diluted with hexanes and the product was collected by filtration to give ethyl mandelimidate hydrochloride salt as a light-yellow solid (110 g, 82% yield): mp 116 °C; MS *m*/*e* 180 $(M + H)^+$; ^{1}H NMR (400 MHz, DMSO-d_6) δ 1.22 (t, J = 6.95 Hz, 3H), 3.64 (bs, 2H), 4.42 (q, J = 6.95 Hz, 2H), 5.51 (s, 1H), 7.38−7.47 (m, 5H). Anal. ($C_{10}H_{13}NO_2$) C, H, N.

Step c. 2-(1,4,5,6-Tetrahydropyrimidyl)phenylmethanol (7; R_1 = H). Into a cold (0 °C) suspension of ethyl mandelimidate hydrochloride salt (52 g, 0.24 mol) in ethanol (250 mL) was added dropwise propane-1,3-diamine (18.1 g, 0.24 mol) over a 10 min period. The new reaction mixture was refluxed for 18 h. Evaporation and crystallization from ethanol and isopropanol gave 2-(1,4,5,6-tetrahydropyrimidyl)phenylmethanol as the hydrochloride salt. The product was dissolved in water (70 mL)

and filtered off. Under cooling, the aqueous solution was basified with NaOH (2.5 N, 30 mL) and the product was collected by filtration to give 2-(1,4,5,6-tetrahydropyrimidyl)-phenylmethanol as a white solid (36.5 g, 80% yield): mp 180 °C; MS *m/e* 191 $(M + H)^+$; ^{1}H NMR (400 MHz, DMSO-d_6) δ 1.53−1.59 (m, 2H), 3.12−3.23 (m, 4H), 4.78 (s, 1H), 6.20 (bs, 2H), 7.27−7.34 (m, 3H), 7.36−7.42 (m, 2H). Anal. ($C_{11}H_{14}N_2O$) C, H, N.

Step d. 2-(1,4,5,6-Tetrahydropyrimidyl) Phenyl Ketone (8; R_1 = H). Into a stirred suspension of 2-(1,4,5,6-tetrahydropyrimidyl)phenylmethanol (28.2 g, 0.15 mol) in methylene chloride (450 mL) was added all at once manganese oxide (50 g, 0.575 mol). The mixture was stirred at room temperature for 48 h. The reaction mixture was filtered through solka floc and washed with chloroform. Evaporation and crystallization from chloroform, ethyl ether, and hexanes gave 2-(1,4,5,6-tetrahydropyrimidyl) phenyl ketone as a light-yellow solid (26.1 g, 85% yield): mp 80 °C; MS *m/e* 189 $(M + H)^+$; ^{1}H NMR (400 MHz, DMSO-d_6) δ 1.6−1.7 (m, 2H), 3.2−3.3 (m, 2H), 3.35−3.46 (m, 2H), 7.09 (brs, 1H), 7.4−7.5 (m, 2H), 7.58−7.62, (m, 1H), 8.02−8.04 (m, 2H). Anal. ($C_{11}H_{12}N_2O$) C, H, N.

Step e. (4-*tert*-Butylphenyl)(phenyl)-1,4,5,6,-tetrahydropyrimidin-2-ylmethanol (10; R_1 = H, R_2 = 4-*tert*-butyl, X = OH). Copper(I) iodide (50 mg) was added at room temperature into a freshly prepared 4-*tert*-butylphenylmagnesium bromide [made by refluxing Mg (0.96 g, 39.31 mmol) and 1-bromo-*tert*-butylbenzene (8.49 g, 39.83 mmol) in THF (40 mL) for 4 h] followed by a solution of 2-(1,4,5,6-tetrahydropyrimidyl) phenyl ketone (3 g, 15.9 mmol) in THF (20 mL). The new reaction mixture was refluxed for 20 h. The volatiles were removed in vacuo, and the residue was taken in aqueous NH_4Cl, acidified with HCl (6 N, 16 mL), and extracted with ethyl ether. The aqueous layer was basified with NH_4OH (30%, 50 mL) and extracted with chloroform. The organic extracts were dried over $MgSO_4$. Evaporation and crystallization from isopropanol gave (4-*tert*-butylphenyl)(phenyl)-1,4,5,6,-tetrahydropyrimidin-2-ylmethanol as a white solid (1.55 g, 30% yield): mp 151 °C; MS *m/e* 323 $(M + H)^+$; ^{1}H NMR (400 MHz, DMSO-d_6) δ 1.27 (s, 9H), 1.6−1.64 (m, 2H) 3.2−3.28 (m, 2H), 3.3−3.35 (m, 2H), 6.6 (bs, 2H), 7.23−7.38 (m, 9H). Anal. ($C_{21}H_{26}N_2O$) C, H, N.

Step f. 2-[(4-*tert*-Butylphenyl)(chloro)phenylmethyl]-1,4,5,6,-tetrahydropyrimidine (11; R_1 = H, R_2 = 4-*tert*-butyl, X = Cl). Into a cold (0 °C) solution of (4-*tert*-butylphenyl)(phenyl)-1,4,5,6-tetrahydropyrimidin-2-ylmethanol (2.7 g, 8.37 mmol) in $CHCl_3$ (10 mL) was added $SOCl_2$ (1.9 mL) over a 10 min period. The reaction mixture was refluxed for 4 h. The volatiles were removed in vacuo, and the residue was taken in benzene and concentrated in vacuo to dryness (twice). Crystallization from chloroform and ethyl ether gave 2-[(4-*tert*-butylphenyl)-(chloro)phenylmethyl]-1,4,5,6-tetrahydropyrimidine as an off-white solid (2.4 g, 84% yield): mp 79 °C; MS *m/e* 341 $(M + H)^+$; ^{1}H NMR (400 MHz, DMSO-d_6) δ 1.26 (s, 9H), 1.88−1.91 (m, 2H), 3.4−3.45 (m, 4H), 7.26 (d, J = 8.66 Hz, 2H), 7.34−7.38 (m, 2H), 7.46−7.49 (m, 5H), 9.42 (bs, 1H). Anal. ($C_{21}H_{25}ClN_2$) C, H, N

Step g. (4-*tert*-Butylphenyl)(phenyl)-1,4,5,6-tetrahydropyrimidin-2-ylmethylamine (12; R_1 = H, R_2 = 4-*tert*-butyl). A solution of 2-[(4-*tert*-butylphenyl)(chloro)phenylmethyl]-1,4,5,6-tetrahydropyrimidine (1 g, 2.65 mmol) in EtOH (5 mL) and freshly prepared EtOH−NH_3 saturated solution (10 mL) were placed in a sealed vessel and stirred at 60 °C for 24 h. The volatiles were removed in vacuo, and the residue was taken in NaOH (2.5 N) and extracted with chloroform. The organic extracts were dried over K_2CO_3. Evaporation gave (4-*tert*-butylphenyl)(phenyl)-1,4,5,6-tetrahydropyrimidin-2-ylmethylamine as a brown, thick oil (0.76 g, 89%). MS *m/e* 322 $(M + H)^+$; ^{1}H NMR (400 MHz, DMSO-d_6) δ 1.29 (s, 9H), 1.87−1.88 (m, 2H), 3.4−3.6 (m, 7H), 7.23 (d, J=8.5 Hz, 2H), 7.34 (d, J=6.9 Hz, 2H), 7.4−7.5 (m, 5H).

Step h. 8-(4-*tert*-Butylphenyl)-8-phenyl-2,3,4,8-tetrahydroimidazol[1,5-*a*]pyrimidin-6-amine (13; R_1 = H, R_2 = 4-*tert*-butyl). A solution of (4-*tert*-butylphenyl)(phenyl)-1,4,5 6-tetrahydropyrimidin-2-ylmethylamine (0.76 g, 2.36 mmol) and cyanogen bromide (1.1 g, 9.45 mmol) in $CHCl_3$ (10 mL) was refluxed for 40 h. The reaction mixture turned into a suspension. The volatiles were removed in vacuo, and the residue was taken in aqueous NH_4Cl (7 mL), basified with NaOH (2.5 N, 7 mL), and extracted with chloroform. The organic extracts were dried over K_2CO_3. Evaporation and purification by flash chromatography on silica gel (CH_2Cl_2/EtOAc/MeOH/Et_3N, 2/2/5.9/0.1) gave **27** as a white solid (75 mg, 9.1% yield): mp 139 °C); MS *m/e* 345 $(M - H)^-$; ^{1}H NMR (400 MHz, DMSO-d_6) δ 1.22 (s, 9H), 1.65−1.68 (m, 2H,), 3.367 (t, J = 5.35 Hz, 2H), 3.5 (t, J = 5.81 Hz, 2H), 6.15 (bs, 2H), 7.2−7.23 (m, 1H), 7.2−7.25 (m, 4H), 7.40 (d, J = 7.64, 2H), 7.52 (d, J = 7.33 Hz, 2H). Anal. ($C_{22}H_{26}N_4$) C, H, N.

General Methods for the Preparation of Compounds Illustrated in Scheme 2. Steps a and b. 1-(3-Bromophenyl)-1-[4-(trifluoromethoxy)phenyl]methanamine (18; R_1 = 4-OCF_3, R_2 = 3-Br). A mixture of magnesium (0.60 g, 24.7 mmol) in THF (6 mL) was heated to 50 °C and treated dropwise with a solution of 1-bromo-4-(trifluoromethoxy)benzene (5.96 g, 24.7 mmol) in THF (18 mL) over a period of 10 min. After being stirred at 50 °C for an additional 1.5 h, the mixture was cooled to room temperature and treated with a solution of 3-bromobenzonitrile (3.0 g, 16.5 mmol) in THF (12 mL). The mixture was then reheated to 65 °C for 1 h. After this time, the reaction mixture was cooled to room temperature and poured into a solution of saturated aqueous ammonium chloride (20 mL) and concentrated ammonium hydroxide (20 mL) at −15 °C and stirred for 5 min. This mixture was then filtered through a pad of Celite with ethyl ether (100 mL). The organic layer of the filtrate was separated, washed with brine (50 mL), and dried over magnesium sulfate. Evaporation of the solvents afforded crude 1-(3-bromophenyl)-1-[4-(trifluoromethoxy)phenyl]methanimine (3.90 g, 68%) as an amber oil. A solution of this crude imine (3.90 g, 11.3 mmol) in MeOH (20 mL) was cooled with an ice bath and treated with sodium borohydride (0.86 g, 22.7 mmol). The cooling bath was removed and the mixture stirred at room temperature for 3 h. After this time the mixture was concentrated and partitioned between NaOH (1 N, 100 mL) and methylene chloride (100 mL). The organic layer was separated and washed with brine (100 mL), dried over potassium carbonate, filtered, and concentrated. Purification by flash chromatography (silica, 1:4 ethyl acetate/hexanes) afforded 1-(3-bromophenyl)-1-[4-(trifluoromethoxy)phenyl]methanamine (1.98 g, 34% over two steps): MS *m/e* 329 $[M - NH_2 + H]^+$; ^{1}H NMR (300 MHz, $CDCl_3$) δ 5.19 (s, 1H), 7.40−7.15 (m, 7H), 7.56 (t, J = 1.7 Hz, 1H). Anal. ($C_{14}H_{11}BrF_3NO$), C, H, N.

Steps c and d. 4-(3-Bromophenyl)-4-[4-(trifluoromethoxy)-phenyl]-1,3-thiazolidine-2,5-dithione (20; R_1 = 4-OCF_3, R_2 = 3-Br). A mixture of 1-(3-bromophenyl)-1-[4-(trifluoromethoxy)-phenyl]methanamine (0.66 g, 1.91 mmol) in methylene chloride (2 mL) and saturated aqueous sodium bicarbonate (2 mL) was cooled with an ice bath, treated with thiophosgene (0.24 g, 2.10 mmol), and stirred vigorously for 30 min. The organic layer was separated, washed with brine (2 mL), dried over sodium sulfate, and concentrated to afford 1-bromo-3-{isothiocyanato[4-(trifluoromethoxy)phenyl]methyl}benzene (0.74 g, 100%) as a yellow oil. A solution of this crude isothiocyanate (0.22 g, 0.567 mmol), carbon disulfide (0.065 g, 0.85 mmol) in tetrahydrofuran (3 mL), was added dropwise into a mixture of potassium *tert*-butoxide (0.07 g, 0.62 mmol) in tetrahydrofuran (2 mL) at −78 °C. The mixture was stirred at −78 °C for 0.5 h, then warmed to room temperature slowly and stirred overnight at room temperature. The mixture was then diluted with ethyl acetate (50 mL) and water (10 mL). The organic layer was separated, washed with brine (10 mL), dried over sodium sulfate, and concentrated to afford

4-(3-bromophenyl)-4-[4-(trifluoromethoxy)phenyl]-1,3-thiazolidine-2,5-dithione (0.86 g, 98%) as a clear oil: MS *m*/*e* 464 $(M + H)^+$; ^{1}H NMR (300 MHz, $CDCl_3$) δ 3.70 (s, br, 1H), 7.86−7.10 (m, 8H).

Step e. 8-(3-Bromophenyl)-8-[4-(trifluoromethoxy)phenyl]-3,4,7,8-tetrahydroimidazo[1,5-*a*]pyrimidine-6(2*H*)-thione (22; R_1 = 4-OCF_3, R_2 = 3-Br). A mixture of 4-(3-bromophenyl)-4-[4-(trifluoromethoxy)phenyl]-1,3-thiazolidine-2,5-dithione (0.60 g, 1.30 mmol) and propane-1,3-diamine (0.40 g, 3.91 mmol) in ethanol (6 mL) was heated at 70 °C for 1.5 h and then cooled to room temperature. The solvents were evaporated, and the residue was partitioned between ethyl acetate (60 mL) and water (30 mL). The organic layer was separated and washed with brine (50 mL), dried over sodium sulfate, filtered, and concentrated. Purification by flash chromatography (silica, 4:1 hexanes/ethyl acetate) afforded 8-(3-bromophenyl)-8-[4-(trifluoromethoxy)phenyl]-3,4,7,8-tetrahydroimidazo[1,5-*a*]pyrimidine-6(2*H*)-thione (0.45 g, 54%) as a white solid: MS *m*/*e* 456 $[M + H]^+$; ^{1}H NMR (300 MHz, $CDCl_3$) δ 3.87 (t, J = 8.5 Hz, 2H), 4.46 (t, J = 8.5 Hz, 2H), 7.59−7.19 (m, 8H), 8.50 (s, 1H).

Step f. 8-(3-Bromophenyl)-8-[4-(trifluoromethoxy)phenyl]-2,3,4,8-tetrahydroimidazo[1,5-*a*]pyrimidin-6-amine (23; R_1 = 4-OCF_3, R_2 = 3-Br). A mixture of 8-(3-bromophenyl)-8-[4-(trifluoromethoxy)phenyl]-3,4,7,8-tetrahydroimidazo[1,5-*a*]pyrimidine-6(2*H*)-thione (0.200 g, 0.438 mmol) and *tert*-butyl hydroperoxide (0.79 g of a 70% solution in water, 8.80 mmol) in methanol (20 mL) and concentrated aqueous ammonium hydroxide (4 mL) was stirred overnight at room temperature. The mixture was then concentrated. Purification by flash chromatography (silica, 95:5:0.25 methylene chloride/methanol/concentrated ammonium hydroxide) afforded 8-(3-bromophenyl)-8-[4-(trifluoromethoxy)phenyl]-2,3,4,8-tetrahydroimidazo-[1,5-*a*]pyrimidin-6-amine (0.16 g, 81%) as a white solid: MS *m*/*e* 453 $[M + H]^+$; ^{1}H NMR (300 MHz, CD_3OD) δ 1.86 (t, J = 5.7 Hz, 2H), 3.47 (t, J = 5.5 Hz, 2H), 3.69 (t, J = 6.0 Hz, 2H), 7.26−7.19 (m, 3H), 7.34−7.30 (m, 1H), 7.46−7.39 (m, 3H), 7.52 (t, J = 1.8 Hz, 1H). Anal. ($C_{19}H_{16}BrF_3N_4O$) C, H, N.

General Methods of Suzuki and Stille Couplings for Compounds Illustrated in Schemes 1 and 2. 8-(3-Pyrimidin-5-ylphenyl)-8-[4-(trifluoromethoxy)phenyl]-2,3,4,8-tetrahydroimidazo[1,5-*a*]pyrimidin-6-amine (24; R_1 = 4-OCF_3, R_2 = 3-Pyrimidin-5-ylphenyl). A mixture of 8-(3-bromophenyl)-8-[4-(trifluoromethoxy)phenyl]-2,3,4,8-tetrahydroimidazo[1,5-*a*]pyrimidin-6-amine (0.25 g, 0.55 mmol), 5-pyrimidineboronic acid (0.082 g, 0.66 mmol), tetrakis(triphenylphosphino)palladium(0) (0.064 g, 0.054 mmol), and potassium carbonate (0.23 g, 1.65 mmol) in 5:1 dioxane/water (7.2 mL) was heated at 100 °C for 3.5 h. The mixture was then cooled to room temperature and concentrated and the crude product purified by flash chromatography (silica, 95:5:0.25 methylene chloride/methanol/concentrated ammonium hydroxide) to 8-(3-pyrimidin-5-ylphenyl)-8-[4-(trifluoromethoxy)phenyl]-2,3,4,8-tetrahydroimidazo[1,5-*a*]pyrimidin-6-amine (**35** entry, Table 2) as a white solid (0.16 g, 60% yield): mp 214−218 °C; MS *m*/*e* 453 $(M + H)^+$; ^{1}H NMR (500 MHz, CD_3OD) δ 1.88 (t, J = 6.5 Hz, 2H), 3.52 (t, J = 6.0 Hz, 2H), 3.71 (t, J = 6.2 Hz, 2H), 7.24 (d, J = 8.2 Hz, 2H), 7.47−7.43 (m, 2H), 7.54−7.51 (m, 2H), 7.69−7.65 (m, 2H), 9.01 (s, 2H), 9.11 (s, 1H). Anal. ($C_{23}H_{19}F_3N_6O$) C, H, N.

8-[3-(2-Fluoropyridin-3-yl)phenyl]-8-[4-(trifluoromethoxy)-phenyl]-2,3,4,8-tetrahydroimidazo[1,5-*a*]pyrimidin-6-amine [24; R_1 = 4-OCF_3, R_2 = 3-(2-fluoropyridin-3-yl)phenyl]. A mixture of 8-(3-bromophenyl)-8-[4-(trifluoromethoxy)phenyl]-2,3,4,8-tetrahydroimidazo[1,5-*a*]pyrimidin-6-amine (0.072 g, 0.159 mmol), 2-fluoro-3-(tributylstannanyl)pyridine (0.092 g, 0.24 mmol), and dichlorobis(triphenylphosphino)palladium(II) (0.006 g, 0.008 mmol) in DMF (2.5 mL) was degassed and then heated at 150 °C in a sealed tube for 1.5 h. The mixture was then cooled to room temperature and diluted with ethyl acetate (50 mL) and 5% aqueous LiCl (20 mL). The organic layer was separated and washed with 5% aqueous LiCl (2 × 10 mL), dried over sodium sulfate, filtered, and concentrated. Purification by flash chromatography (silica, 95:5:0.25 methylene chloride/methanol/concentrated ammonium hydroxide) afforded 8-[3-(2-fluoropyridin-3-yl)phenyl]-8-[4-(trifluoromethoxy)phenyl]-2,3,4,8-tetrahydroimidazo[1,5-*a*]pyrimidin-6-amine (**37** entry; Table 2) as a white solid (0.042 g, 56% yield): mp 120−125 °C; MS *m*/*e* 470 $(M + H)^+$; ^{1}H NMR (500 MHz, CD_3OD) δ 1.87 (m, 2H), 3.48 (m, 2H), 3.69 (t, J = 5.9 Hz, 2H), 7.23 (d, J = 8.7 Hz, 2H), 7.49−7.37 (m, 6H), 7.53 (m, 1H), 8.04−7.98 (m, 1H), 8.15 (dd, J = 4.8, 1.1 Hz, 1H). Anal. ($C_{24}H_{19}F_4N_5O$) C, H, N.

Generation of the Enantiomers of Key Compounds Using Chiral HPLC Techniques. (8*R*)-8-(3-Pyrimidin-5-ylphenyl)-8-[4-(trifluoromethoxy)phenyl]-2,3,4,8-tetrahydroimidazo[1,5-*a*]pyrimidin-6-amine [(*R*)-35] and (8*S*)-8-(3-Pyrimidin-5-ylphenyl)-8-[4-(trifluoromethoxy)phenyl]-2,3,4,8-tetrahydroimidazo[1,5-*a*]pyrimidin-6-amine [(*S*)-35]. Racemic 8-(3-pyrimidin-5-ylphenyl)-8-[4-(trifluoromethoxy)phenyl]-2,3,4,8-tetrahydroimidazo-[1,5-*a*]pyrimidin-6-amine (1.30 g, 2.87 mmol) was separated into its enantiomers using a Chiralpak AD 5 cm × 50 cm column (90:10:0.1 heptane/ethanol/diethylamine). The first eluting peak (t_R = 35 min) was collected and concentrated to give a pale-yellow oil. The residue was redissolved in a minimal amount of methylene chloride, and a solid was precipitated by the addition of hexanes. This solid was collected by filtration and dried under vacuum for 24 h to afford (*R*)-**35** as an off-white solid (0.55 g): R_f = 0.38 (95:5:0.25 methylene chloride/methanol/concentrated ammonium hydroxide); mp 128−131 °C; $[\alpha]^{25}_D$ −10.1° (*c* 0.50, MeOH); MS *m*/*e* 453 $(M + H)^+$; ^{1}H NMR (300 MHz, CD_3OD) δ 1.91(t, J = 5.7, 5.4 Hz, 2H), 3.55 (t, J = 5.4 Hz, 2H), 3.75 (t, J = 5.7 Hz, 2H), 7.26 (d, J = 8.7 Hz, 2H), 7.48−7.44 (m, 2H), 7.57−7.51 (m, 2H), 7.70−7.67 (m, 2H), 9.02 (s, 2H) 9.12 (s, 1H). HPLC (Chiralpak AD analytical column) >99% (AUC), t_R = 15.44 min. Anal. ($C_{23}H_{19}F_3N_6O$) C, H, N.

The second eluting peak (t_R = 48 min) was collected and concentrated to give a pale-yellow oil. The oil residue was redissolved in a minimal amount of methylene chloride and then triturated with hexanes and filtered. The product was dried under vacuum for 24 h to afford (*S*)-**35** as an off-white solid (0.58 g): R_f = 0.38 (95:5:0.25 methylene chloride/methanol/concentrated ammonium hydroxide); mp 123−130 °C; $[\alpha]^{25}_D$ +9.9° (*c*, 0.50, MeOH); MS *m*/*e* 453 $(M + H)^+$; ^{1}H NMR (300 MHz, CD_3OD) δ 1.91 (tt, J = 5.7, 5.4 Hz, 2H), 3.55 (t, J = 5.4 Hz, 2H), 3.75 (t, J = 5.7 Hz, 2H), 7.26 (d, J = 8.7 Hz, 2H), 7.46−7.48 (m, 2H), 7.51−7.57 (m, 2H), 7.67−7.70 (m, 2H), 9.02 (s, 2H), 9.12 (s, 1H). HPLC (Chiralpak AD analytical column) >99% (AUC), t_R = 19.11 min. Anal. ($C_{23}H_{19}F_3N_6O$) C, H, N.

(8*R*)-8-[3-(2-Fluoropyridin-3-yl)phenyl]-8-[4-(trifluoromethoxy)phenyl]-2,3,4,8-tetrahydroimidazo[1,5-*a*]pyrimidin-6-amine [(*R*)-37] and (8*S*)-8-[3-(2-fluoropyridin-3-yl)phenyl]-8-[4-(trifluoromethoxy)phenyl]-2,3,4,8-tetrahydroimidazo[1,5-*a*]pyrimidin-6-amine [(*S*)-37]. A racemic mixture of 8-[3-(2-fluoropyridin-3-yl)phenyl]-8-[4-(trifluoromethoxy)phenyl]-2,3,4,8-tetrahydroimidazo[1,5-*a*]pyrimidin-6-amine (0.74 g, 1.57 mmol) was placed on a Chiralpak AD 5 cm × 50 cm column (90:10:0.1 heptane/ethanol/diethylamine as eluent). The first eluting peak (t_R = 19 min) was collected and concentrated to a pale-yellow oil. The oil residue was redissolved in a minimal amount of methylene chloride, triturated with hexanes, and filtered. The filter cake is dried under vacuum for 24 h to (*S*)-**37** as an off-white solid (0.315 g): R_f = 0.49 (90:10:0.5 methylene chloride/methanol/concentrated ammonium hydroxide); mp 124−128 °C; $[\alpha]^{25}_D$ +12.6° (*c* 0.5, MeOH); MS *m*/*e* 470 $(M + H)^+$; ^{1}H NMR (500 MHz, CD_3OD) δ 1.90−1.85 (m, 2H), 3.49 (t, J = 5.4 Hz, 2H), 3.70 (t, J = 6.0 Hz, 2H), 7.23 (d, J = 8.2 Hz, 2H), 7.40−7.37 (m, 1H), 7.44−7.41 (m, 1H), 7.49−7.45 (m, 3H), 7.55−7.52 (m, 1H), 7.58 (s, 1H), 8.03−7.98 (m, 1H), 8.16 (dd, J = 4.8, 1.1 Hz, 1H). HPLC (Chiralpak AD analytical column) >99% (AUC), t_R = 8.47 min. Anal. ($C_{24}H_{19}F_4N_5O$) C, H, N.

The second eluting peak (t_R = 26 min) was collected and concentrated to a pale-yellow oil. The oil residue is redissolved

in a minimal amount of methylene chloride, triturated with hexanes, and filtered. The filter cake is dried under vacuum for 24 h to afford (*R*)-**37** as an off-white solid, 0.299 g; $R_f = 0.49$ (90:10:0.5 methylene chloride/methanol/concentrated ammonium hydroxide): mp 128−131 °C; $[\alpha]^{25}_D$ −11.6° (*c* 0.5, MeOH); MS *m*/*e* 470 $(M + H)^+$; ^{1}H NMR (500 MHz, CD_3OD) δ 1.85−1.91 (m, 2H), 3.51 (t, $J = 5.3$ Hz, 2H), 3.72 (t, $J = 6.0$ Hz, 2H), 7.25 (d, $J = 8.2$ Hz, 2H), 7.37−7.40 (m, 1H), 7.42−7.44 (m, 1H), 7.45−7.49 (m, 3H), 7.53−7.57 (m, 1H), 7.58 (d, $J = 1.4$ Hz, 1H), 8.03−7.98 (m, 1H), 7.58 (s, 1H), 8.16 (dd, $J = 4.8$, 1.1 Hz, 1H). HPLC (Chiralpak AD analytical column) >99% (AUC), $t_R = 11.91$ min. Anal. ($C_{24}H_{19}F_4N_5O$) C, H, N.

Biological Methods. FRET-Based Peptide Cleavage Assays. A homogeneous, continuous fluorescence resonance energy transfer (FRET) was used to assess compound inhibition for BACE1, BACE2, cathepsin D, pepsin, and renin activities.[30] The BACE1 and BACE2 activities were based on the cleavage of peptide substrate Abz-SEVNLDAEFR-Dpa (Swedish substrate), while peptide substrate MOCAc-GKPILFFRLK (Dnp)-D-R-NH_2 was used for cathepsin D and pepsin, and peptide substrate RE(EDANS)-IHPFHLVIHTK(DABCYL)-R was used for renin. Kinetic rates were calculated, and IC_{50} values were determined by fitting the % inhibition as a function of compound concentration to the Hill equation $(y = [(BKn) + (100 \times xn)]/(Kn + xn)$.

Cell-Based Aβ Inhibition Assay. CHO-K1 cells recombinantly expressing human wild-type APP (CHO-WT) were grown to confluence and then treated with serum-free medium (Ultraculture) supplemented with test compound in DMSO or DMSO alone (vehicle) at a final [DMSO] of 0.1% (v/v). Conditioned medium was harvested at 24 h and assayed using streptavidin MSD plates and an electrochemiluminescent immunoassay with biotinylated mouse monoclonal antibody 6E10 (Signet, Dedham, MA) as capture, and rabbit anti-Aβ_{40} or Aβ_{42} antibodies (Biosource, Camarillo, CA) as detection antibodies, with a secondary of MSD ECL tagged sheep antirabbit for electrochemiluminescent amplification.

Data analysis of the MSD assay was performed by fitting the percent inhibition as a function of compound concentration to a four-parameter logistic curve, and the concentration at which the cellular production of Aβ_{40} or Aβ_{42} was reduced by 50% (EC_{50}) was determined. Compound toxicity was assessed via mitochondrial function using an MTS readout (MTS kit from Promega); values are represented as LD_{50} or the dose of compound that resulted in 50% of control signal (e.g., 50% of the highest MTS signal).

X-ray Crystallography. Cloning/Expression of BACE1. A human BACE1 secreting mammalian secreting cell line (CHO cell line) was made by expressing a construct in which the prodomain plus ectodomain of human BACE1 (residues 22−454) was fused to the honeybee melittin secretory leader sequence at the 5′ end, and the Fc region of IgG, separated from the BACE sequence via an enterokinase cleavage site, was fused at the 3′ end of BACE1. The BACE1/Fc fusion protein was affinity purified by protein-A sepharose, and removal of the Fc domain was achieved with enterokinase cleavage. Purified BACE1 protein was accomplished via sequential size-exclusion chromatography. *E. coli* derived expression material was used for cocrystallographic studies. A codon-derived BACE1 *E. coli* expression construct was fused to a carboxy terminal 6X HIS tag. After scale-up, inclusion bodies were purified and protein was refolded and dialyzed. The pro domain was cleaved with furin, and BACE1 was further purified by size exclusion chromatography. The refolded *E. coli* derived BACE1 showed the same enzymatic activity as the CHO-derived material (data not shown).

Crystallization and X-ray Diffraction Analysis of BACE1. BACE1/**3** complex was resolved through cocrystallization. The BACE1 costructure with **3** revealed the relatively open-conformation state of the flap compared with the apo BACE1 crystals. The ligand induced conformational change on the flap region was observed. Data were collected at the Advanced Light Source, station 5.0.2, on a ADSC Quantum-4 detector and reduced with HKL-2000.

Molecular Modeling. Docking calculations were performed using the QXP software package.[31] Once the X-ray ligands were minimized in the active site, constrained simulated annealing calculations were performed to relieve any artifacts of the X-ray refinement perceived as unfavorable interactions or strain by the modified AMBER force field with QXP. The X-ray ligand was then redocked to confirm that the lowest energy pose is in agreement with the X-ray structure. Once the binding site model was generated, docking of analogues was performed using the QXP Monte Carlo docking algorithm mcdock in combination with CombiDOCK. Visualization of X-ray structures and docking results was performed using the InsightII software package (www.accelrys.com, Accelrys, Inc., San Diego, CA). Conformational analysis was performed using Macromodel (Macromodel 8.0; Schrodinger, LLC, Portland, OR), with the OPLS-AA force fields, and a GBSA solvation model.

Supporting Information Available: X-ray crystallographic data (collection details, refinement statistics), ^{1}H NMR and analytical data of intermediates and final compounds not listed in the Experimental Section, and additional information of biological assays. This material is available free of charge via the Internet at http://pubs.acs.org.

References

(1) Selkoe, D. J. Alzheimer disease: genotypes, phenotypes, and treatments. *Science* **1977**, *275*, 630–631.
(2) Hardy, J. The Alzheimer family of diseases: many etiologies, one pathogenesis? *Proc. Natl. Acad. Sci. U.S.A.* **1997**, *94*, 2095–2097.
(3) Vassar, R.; Citron, M. Aβ-generating enzymes: recent advances in β- and γ-secretase research. *Neuron* **2000**, *27*, 419–422.
(4) Selkoe, D. J. Alzheimer's disease: genes, proteins, and therapy. *Physiol. Rev.* **2001**, *81*, 741–766.
(5) Hussain, I.; Powell, D.; Howlett, D. R.; Tew, T. g.; Meek, T. D.; Chapman, C.; Gloger, I. S.; Murphy, K. E.; Southan, C. D.; Ryan, D. M.; Smith, T. S.; Simmons, D. L.; Walsh, F. S.; Dingwall, C.; Christie, G. Identification of a novel aspartic protease (Asp2) as β-secretase. *Mol. Cell. Neurosci.* **1999**, *14*, 419–427.
(6) Lin, X.; Koelsch, G.; Wu, S.; Downs, D.; Dashti, A.; Tang, J. Human aspartic protease memapsin 2 cleaves the β-secretase site of β-amyloid precursor protein. *Proc. Natl. Acad. Sci. U.S.A.* **2000**, *97*, 1456–1460.
(7) Vassar, R.; Bennett, B. D.; Babu-Khan, S.; Kahn, S.; Mendiaz, E. A.; Denis, P.; Teplow, D. B.; Ross, S.; Amarante, P.; Loeloff, R.; Luo, Y.; Fischer, S.; Fuller, J.; Edenson, S.; Lile, J.; Jarosinski, M. A.; Biere, A. L.; Curran, E.; Burgess, T.; Louis, J.-C.; Collins, F.; Treanor, J.; Rogers, G.; Citron, M. β-Secretase cleavage of Alzheimer's amyloid precursor protein by transmembrane aspartic protease BACE. *Science* **1999**, *286*, 735–741.
(8) Ghosh, A.; Kumaragurubaran, N.; Tang, J. Recent developments of structure-based β-secretase inhibitor's for Alzheimer's disease. *Curr. Top. Med. Chem.* **2005**, *5*, 1609–1622.
(9) Cumming, J. N.; Iserloh, U.; Kennedy, M. E. Design and development of BACE1 inhibitors. *Curr. Opin. Drug Discovery Dev.* **2004**, *7*, 536–556.
(10) Durham, T. B.; Shepherd, T. A. Progress toward the discovery and development of efficacious BACE inhibitors. *Curr. Opin. Drug Discovery Dev.* **2006**, *9*, 776–791.
(11) Baxter, E. W.; Reitz, A. B. BACE inhibitors for the treatment of Alzheimer's disease. *Annu. Rep. Med. Chem.* **2005**, *40*, 35–48.
(12) Schmidt, B.; Baumann, S.; Braub, H. A.; Larbig, G. Inhibitors and modulators of β- and γ-secretase. *Curr. Top. Med. Chem.* **2006**, *6*, 377–392.
(13) Guo, T.; Hobbs, D. W. Development of BACE1inhibitors for Alzheimer's disease. *Curr. Med. Chem.* **2006**, *13*, 1811–1829.
(14) John, V.; Beck, J. P.; Bienkowski, M. J.; Sinha, S.; Heinrikson, R. l. Human β-secretase (BACE) and BACE inhibitors. *J. Med. Chem.* **2003**, *46*, 4625–4630.
(15) Carmen Villaverde, M.; Gonzalez-Louro, L.; Sussman, F. The search for drug leads targeted to the β-secretase: an example of the roles of computer assisted approaches in drug discovery. *Curr. Top. Med. Chem.* **2007**, *7*, 980–990.

(16) Hong, L.; Koelsch, L. X.; Wu, S.; Terzyan, S.; Ghosh, A.; Zhang, X. C.; Tang, J. Structure of the protease domain of memapsin 2 (β-secretase) complexed with inhibitor. *Science* **2000**, *290*, 150–153.
(17) Stachel, S. J.; Coburn, C. A.; Steele, T. G.; Jones, K. G.; Loutzenhiser, E. F.; Gregro, A. R.; Rajapakse, H. A.; Lai, M.-T.; Crouthamel, M.-C.; Xu, M.; Tugusheva, K.; Lineberger, J. E.; Pietrak, B. L.; Espeseth, A. S.; Shi, X.-P.; Chen-Dodson, E.; Holloway, M. K.; Munshi, S.; Simon, A. J.; Kuo, L.; Vacca, J. P. Structure-based design of potent and selective cell-permeable inhibitors of human β-secretase (BACE1). *J. Med. Chem*. **2004**, *47*, 6447–6450.
(18) Coburn, C. A.; Stachel, S. J.; Li, Y.-M.; Rush, D. M.; Steele, T. G.; Chen-Dodson, E.; Holloway, M. K.; Xu, M.; Huang, Q.; Lai, M.-T.; DiMuzio, J.; Crouthamel, M.-C.; Shi, X.-P.; Sardana, V.; Chen, Z.; Munshi, S.; Kuo, L.; Makara, G. M.; Annis, D. A.; Tadikonda, P. K.; Nash, H. M.; Vacca, J. P. Identification of a small molecule nonpeptide active site β-secretase inhibitor that displays a non-traditional binding mode for aspartyl proteases. *J. Med. Chem*. **2004**, *47*, 6117–6119.
(19) Garino, C.; Pietrancosta, N.; Laras, Y.; Moret, V.; Rolland, A.; Quelever, G.; Kraus, J.-L. BACE1 inhibitory activities of new substituted phenyl-piperazine coupled to various heterocycles: chromene, coumarin, and quinoline. *Bioorg. Med. Chem. Lett*. **2006**, *16*, 1995–1999.
(20) Huang, D.; Luthi, U.; Kolb, P.; Cecchine, M.; Barberis, A.; Caflisch, A. In silico discovery of β-secretase inhibitors. *J. Am. Chem. Soc*. **2006**, *128*, 5436–5443.
(21) Huang, D.; Luthi, U.; Kolb, P.; Edler, K.; Cecchine, M.; Audedat, S.; Barberis, A.; Caflisch, A. Discovery of cell-permeable nonpeptide inhibitors of β-secretase by high-throughput docking and continuum electrostatics calculations. *J. Med. Chem*. **2005**, *48*, 5108–5111.
(22) Rajapaske, H. A.; Nantermet, P. G.; Selnick, H. G.; Munshi, S.; McGaughey, G. B.; Lindsley, S. R.; Young, M. B.; Lai, M.-T.; Espeseth, A. S.; Shi, X.-P.; Colussi, D.; Pietrak, B.; Crouthamel, M.-C.; Tugusheva, K.; Huang, Q.; Simon, A. J.; Kuo, L.; Hazuda, D. J.; Graham, S.; Vacca, J. P. Discovery of oxadiazoyl tertiary carbinamine inhibitors of β-secretase (BACE1). *J. Med. Chem*. **2006**, *49*, 7270–7273.
(23) Edwards, P. D.; Albert, J. S.; Sylvester, M.; Aharony, D.; Andisik, D.; Callaghan, O.; Campbell, J. B.; Carr, R. A.; Chessari, G.; Congreve, M.; Frederickson, M.; Folmer, R. H.; Geschwindner, S.; Koether, G.; Kolmodin, K.; Krumrine, J.; Mauger, R. C.; Murray, C. W.; Olsson, L.; Patel, S.; Spear, N.; Tian, G. Application of fragment-based lead generation to the discovery of novel, cyclic amidine β-secretase inhibitors with nanomolar potency, cellular activity and high ligand efficiency. *J. Med. Chem*. **2007**, *50*, 5912–5925.
(24) Murray, C, W.; Callaghan, O.; Chessari, A.; Congreve, M.; Frederickson, M.; Hartshorn, M. J.; McMenamin, R.; Patel, S.; Wallis, N. Application of fragment screening by X-ray crystallography to β-secretase. *J. Med. Chem*. **2007**, *50*, 1116–1123.
(25) Congreve, M.; Aharony, D.; Albert, J.; Callaghan, O.; Campbell, J.; Carr, R. A. E.; Chessari, G.; Cowan, S.; Edwards, P. D.; Frederickson, M.; McMenamin, R.; Murray, C. W.; Patel, S.; Wallis, N. Application of fragment screening by X-ray crystallography to the discovery of aminopyridines as inhibitors of β-secretase. *J. Med. Chem*. **2007**, *50*, 1124–1132.
(26) Geschwindner, S.; Olsson, L.-L.; Albert, J.; Deinum, J.; Edwards, P. D.; de Beer, T.; Folmer, R. H. A. Discovery of a novel warhead against β-secretase through fragment-based lead generation. *J. Med. Chem*. **2007**, *50*, 5903–5911.
(27) Cole, D. C.; Manas, E.; S.; Stock, J. R.; Condon, J. S.; Jennings, L. D.; Aulabaugh, A.; Chopra, R.; Cowling, R.; Ellingboe, J. W.; Fan, K. Y.; Harrison, B. L.; Hu, Y.; Jacobsen, S.; Jin, G.; Lin, L.; Lovering, F. E.; Malamas, M. S.; Stahl, J.; Strand, J.; Sukhedo, M. N.; Svenson, K.; Turner, M. J.; Wagner, E.; Wu, J.; Zhou, P.; Bard, J. Acylguanidines as small-molecule β-secretase inhibitors. *J. Med. Chem*. **2006**, *49*, 6158–6161.
(28) Stille, J. K. The palladium-catalyzed cross-coupling reactions of organotin reagents with organic electrophiles. *Angew. Chem., Int. Ed. Engl*. **1986**, *25*, 508–524.
(29) Miyaura, N.; Suzuki, A. Palladium-catalyzed cross-coupling reactions of organoboron compounds. *Chem. Rev*. **1995**, *95*, 2457–2483.
(30) Wu, P.; Brand, L. Resonance energy transfer: methods and applications. *Anal. Biochem*. **1994**, *218*, 1–13.
(31) McMartin, C.; Bohacek, R. S. *J. Comput.-Aided Mol. Des*. **1997**, *11*, 333–344.
(32) Hsiao, K.; Chapman, P.; Nilsen, S.; Eckman, C.; Harigaya, Y.; Younkin, S.; Yang, F.; Cole, G. Correlative memory deficits, Abeta elevation, and amyloid plaques in transgenic mice. *Science* **1996**, *274*, 99–102.